Scripta Materialia 194 (2021) 113684

Contents lists available at ScienceDirect

Scripta Materialia

journal homepage: www.elsevier.com/locate/scriptamat

Humidity-dependent flaw sensitivity in the crack propagation resistance of 3D-printed nano-ceramics

Edoardo Rossi[a], Jens Bauer[b,*], Marco Sebastiani[a,*]

[a] Engineering Department, "Roma TRE" University, Via della Vasca Navale 79, Rome 00146, Italy
[b] Mechanical and Aerospace Engineering Department, University of California, Irvine, CA 92697, USA

ARTICLE INFO

Article history:
Received 16 November 2020
Revised 8 December 2020
Accepted 17 December 2020
Available online 30 December 2020

Keywords:
Two-photon polymerization direct laser writing
Pyrolytic carbon
Fracture toughness
Pillar splitting
Humidity

ABSTRACT

3D-printed nano-architected ceramic metamaterials currently emerge as a class of lightweight materials with exceptional strength and stiffness. However, their application is hampered by the lack of knowledge on their mechanical reliability. Characteristics like the fracture strength and their dependency on environmental conditions are unknown. We herein present and discuss a nanoindentation pillar splitting method to measure fracture toughness, elastic modulus, and hardness of 3D-printed nano-ceramics. We show that two photon polymerization-derived pyrolytic carbon achieves improved fracture toughness over macroscopic forms of vitreous carbon, with values up to 3.1 $MPam^{0.5}$. However, experiments at different humidity levels reveal that only few, nanometer-sized, surface cavities can cause embrittlement from liquid diffusion, which promotes earlier crack propagation. While comparable effects are less relevant in macro-size ceramics, this study demonstrates that reliability and durability of micro- and nano-architected ceramic metamaterials and devices requires toughening design approaches that focus on size-dependent surface effects.

Pyrolysis of 3D-printed polymeric structures has been shown highly effective to synthesize complex carbon nano-ceramics with exceptional mechanical strength and feature-sizes well below the capabilities of the highest-resolution 3D additive manufacturing techniques alone [1]. Over the last decades, the evolution of high-precision 3D-printing techniques, like two-photon polymerization direct laser writing (TPP-DLW) [2,3], dramatically accelerated a wide range of research and engineering fields [4–9]. As these techniques are generally limited to polymers, material conversion post-processing is applied to create ceramic and metallic parts [5]. In particular, pyrolysis conversion routes are increasingly adopted to additively manufacture carbon [1,11,12], as well as silicon-based [10,13,14] structures due to the straightforward process and the resulting superior material properties.

Despite the increasing application of additively manufactured pyrolytic nano-ceramics, few studies are investigating their intrinsic mechanical properties [12,14,15]: measured properties are limited to strength and stiffness. Other important characteristics, like hardness and fracture toughness, which are of central relevance for ceramics, are unknown. Furthermore, the mechanical behavior of additively manufactured pyrolytic carbon can be complex [15,16], and the effects of processing [17–19] and environmental testing conditions [20], including relative humidity (RH), need to be investigated for a thorough understanding.

For macroscopic glass ceramics, deleterious humidity effects on the fracture strength have been widely investigated and are a result of the concurrent action of multiple effects, including stress-enhanced chemical reactions between the Si–O–Si bond and water at the crack tip [21,22]. Using the double-cleavage-drilled-compression method in a humid environment (50-56%) [23] an early study showed that different crack propagation velocities can be observed for different fictive temperatures of the glass, confirming that water from the environment reacts with the glass to promote crack growth [24].

Opposed to silica and soda-lime glasses, only few studies elucidate humidity effects on pyrolytic glassy carbon [25,26], showing less sensitivity to static fatigue in water. In the same works, glassy carbons with higher elastic modulus are shown to be more resistant to subcritical crack growth [25]. Currently, there are no studies on how humidity effects should be considered when designing pyrolytic micro- and nano-architected glass ceramics [1,13,14,27],

* Corresponding authors.
E-mail addresses: jens.bauer@uci.edu (J. Bauer), marco.sebastiani@uniroma3.it (M. Sebastiani).

https://doi.org/10.1016/j.scriptamat.2020.113684

where the characteristic dimension of individual structure elements, like beam diameters, can be as small as <200 nm.

In this study, we characterized the fracture toughness of TPP-DLW-derived pyrolytic carbon via nanoindentation micro-pillar splitting depending on the material's surface flaw distribution and the environmental humidity. While this property is typically difficult to determine at small scales, nanoindentation micro-pillar splitting has recently been demonstrated as an effective way to overcome experimental complications [28]. In contrast to established small-scale fracture toughness experiments, which typically involve elaborate and invasive specimen preparation techniques, such as focused ion beam (FIB) milling, the here adopted combination of 3D-printing and pillar splitting allowed for the straightforward analysis of a statistically relevant number of specimens.

This technique involves the indentation of micro-pillars until fracture occurs and does not require any post-test measurement of crack lengths [28–30]. The simple relationship

$$K_c = \gamma \frac{P_c}{R^{3/2}} \quad (1)$$

thereby calculates the fracture toughness, K_c, with the material-dependent dimensionless constant, γ, the load at which the failure by splitting occurs, P_c, and the pillar radius, R. γ solely depends on the material's hardness-to-elastic-modulus ratio, its Poisson's coefficient and the indenter tip geometry, and has recently been determined for a wide range of material and tip combinations via cohesive zone finite element modeling [28–30]. In a previous study, the effect of pillar diameter on measured fracture toughness was investigated [29] to confirm that γ is not dependent on the pillar size, when microstructural features (e.g. grain size) are significantly smaller than pillar diameter. Herein, this is the case, as we tested amorphous pyrolytic carbon pillars with diameter of about 6 µm. When testing the same material under different conditions the ratio between critical loads (P_c) directly provides information on the variation of the crack propagation resistance, independently from the calibration coefficient, $\boldsymbol{\gamma}$.

Pyrolytic carbon micro-pillars were manufactured via two-photon polymerization direct laser writing (TPP-DLW) and subsequent pyrolysis [1]. TPP-DLW was performed using a Photonic Professional GT (Nanoscribe GmbH & Co. KG) system equipped with a Plan-Apochromat 63 × 1.4 Oil DIC M27 (Carl Zeiss AG) objective and a FemtoFiber pro NIR (TOPTICA Photonics AG) laser [31]. Polymeric templates were printed from the photoresist Ip-Dip (Nanoscribe GmbH & Co. KG) on silicon substrates in a layer-by-layer sequence using the TPP-DLW system's galvanometric mirror scanning mode, with a laser average power of 19 mW and a writing speed of 20,000 µm/s. Uniform circular pillars with a height-to-diameter ratio of two and nominal diameters of 20 µm, and 40 µm, respectively, were manufactured in a [0/60/120/90/150/30] laminate manner from unidirectional layers, consisting of multiple voxel-lines with a hatching distance, and a slicing distance between neighboring layers of 0.1 µm and 0.2 µm, respectively. After TPP-DLW, samples were submerged in propylene glycol monomethyl ether acetate (PGMEA) for 20 min, to dissolve uncured photoresist, followed by a 5 min-long isopropanol bath for further cleaning. Subsequently, samples were dried using a CPD300 (Leica Microsystems GmbH) critical point dryer. The polymeric templates were then pyrolyzed to carbon at 900°C for 1 hour in a vacuum tube furnace, with a maximum ramp rate of 3°C/min [1]. During pyrolysis, all specimens underwent linear isotropic shrinkage of approximately 70%, resulting in pyrolytic carbon micro-pillars with average diameters of 5.3 µm and 11.8 µm, respectively, as measured via scanning electron microscopy (SEM) imaging with a FEI Helios NanoLab^{TM} 600 dual beam microscope. Surface and internal flaw distribution were investigated via SEM and scanning transmission electron microscopy (STEM), respectively.

Mechanical characterization of the pyrolytic carbon micro-pillars was conducted with a G200 Keysight nanoindentation system equipped with a standard Berkovich diamond tip (Micro Star Technologies, Huntsville, TX, USA) with a centerline-to-face angle of 65.3°. To exclude tip positioning uncertainty [32] only experiments where the indenter tip was centered on the pillar surface, with a minimum position accuracy of 0.5 µm, were considered. This was confirmed via post-experiment SEM observations of residual marks on the substrate. Elastic modulus (E) and hardness (H) were determined via continuous stiffness measurement (CSM) on the top surface of the 11.8 µm-diameter micro-pillars. Before and after each test the tip was calibrated on a certified fused quartz reference sample. To minimize boundary effects the maximum indentation depth was set to 150 nm, equal to ~1/80 of the pillar diameter, and E and H values were extracted at an indentation depth of 100 nm. A Poisson's ratio of 0.17 was used for the elastic modulus calculations [33]. Only tests made on pillars that were free of surface flaws were considered.

Nanoindentation pillar splitting of the 5.3 µm-diameter micro-pillars at a constant strain rate of 0.05 sec^{-1} was used to evaluate the fracture toughness of the TPP-DLW-derived pyrolytic carbon. The specific calibration coefficient for the present material was calculated by polynomial interpolation of the γ versus H/E-ratio function, which has been established by the authors in a previous publication [29]. The effect of RH on the fracture toughness of the micro-pillars was investigated for two extreme RH ranges. Humid air was used to adjust RH to >60% and RH of <5% was achieved by replacing the environmental air within the instrument sealed cabinet with dry nitrogen at room pressure. The RH was measured by an analog artificial fiber hygrometer.

To investigate the impact of pyrolysis induced flaws on the fracture toughness of TPP-DLW-derived pyrolytic carbon, we characterized micro-pillar specimens with and without detectable surface flaws. Fig. 1a and b show SEM micrographs of representative pristine and surface flaw-containing specimens, respectively. The lateral dimensions of detected surface flaws were measured to be in the range of 200-500 nm. Independently from the surface condition, STEM analysis of a diametric vertical cross-section, extracted via FIB milling (Fig. 1c) revealed no detectible internal defects or porosity, as well as a completely amorphous microstructure.

Fig. 2 compares the nanoindentation behavior, reporting the elastic modulus (E) and hardness (H) depth profile measurements, at RH <5% and RH >60%, as obtained from 11.8 µm diameter pyrolytic carbon micro-pillars. Independent from RH, average values of E=46.9±4.2 GPa and H=7.7±1.4 GPa were found. The reported values of elastic modulus and hardness served as input for the polynomial interpolation of the γ versus H/E-ratio function [29] for the determination of the dimensionless coefficient (γ). For the pyrolytic carbon and the Berkovich indenter of this study, the computed gamma coefficient was 0.16±0.1.

Fig. 3 shows the splitting experiments with the pyrolytic carbon micro-pillars and the corresponding results. A representative arrangement of the splitting procedure with a specimen with surface flaws is given in Fig. 3a. Indentation marks just before fracture, after the specimen has been loaded to 50 mN, showed the presence of surface concentric ring cracks (Fig. 3b), as characteristic for glassy carbon [34]. Focused ion beam cross-sectional analysis of the residual indentation imprints revealed the presence of pronounced median cracks (Fig. 3c). The considerably larger size compared to the concentric ring cracks, which were observed from the top-view, suggests median cracks are the main driving force for unstable failure. Ring cracks had a 45° orientation, consistent with the shear deformation of the material in the indentation volume. A video of a FIB tomography is available in the supplementary material. While the specimens fully fragmented during fracture, post-mortem SEM micrographs confirmed proper inden-

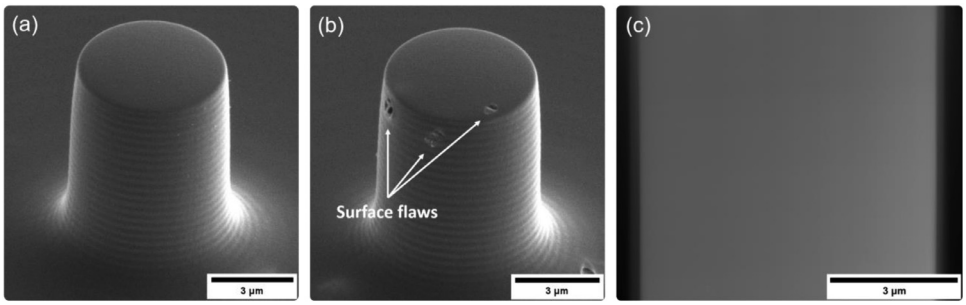

Fig. 1. Representative SEM micrographs of pyrolytic carbon micro-pillars (a) without and (b) with observable surface flaws, respectively. Images are acquired at 52° tilt. (c) STEM micrograph of a lamella extracted from the diametric vertical cross-section of a pillar.

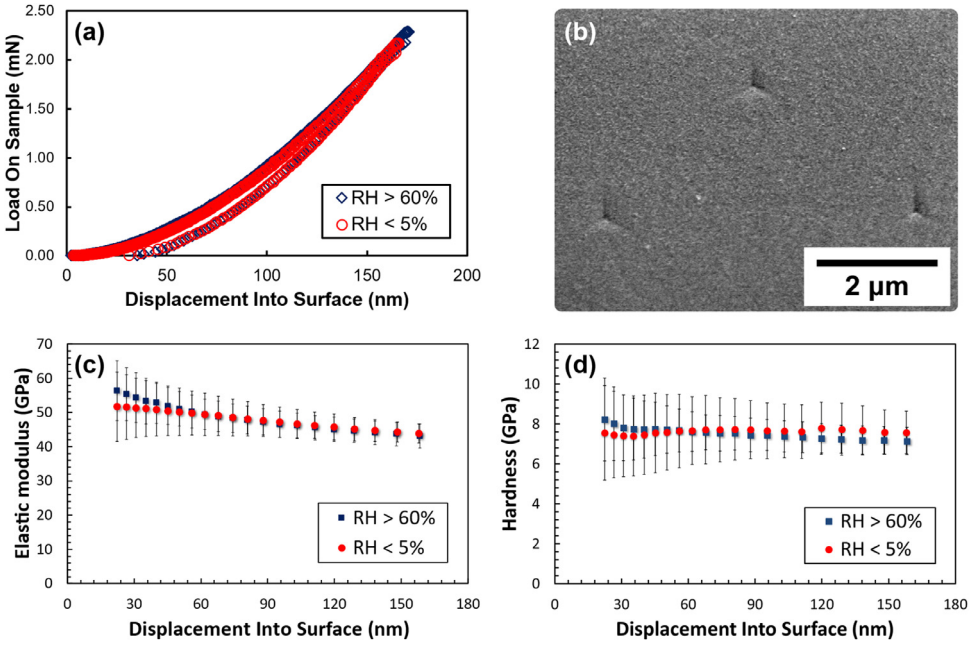

Fig. 2. Nanoindentation continuous stiffness measurements (CSM) performed on ~12 µm-diameter pyrolytic carbon micro-pillars. (a) Representative load – depth curves and (b) residual Berkovitch imprints alongside (c) elastic modulus – depth profiles and (d) hardness – depth profiles at relative humidity (RH) values of <5% and >60%.

ter positioning via the residual Berkovich imprint on the specimen substrate. Fig. 3d and e show load-displacement curves for pristine structures and specimens with surface defects measured at RH values of <5% and >60%, respectively. In all cases, a clear displacement burst was observed corresponding to failure via unstable crack propagation. Independent from the surface quality, experiments showed good reproducibility at RH <5%, with splitting loads of 74.9±8.8 mN, corresponding to calculated K_c values of 2.80±0.3 MPam$^{0.5}$. In contrast, splitting loads at RH >60% were significantly affected by the testing humidity with notably increased scatter and decreased average values of 64.1±15.6 mN; average K_c value of 2.27±0.6 MPam$^{0.5}$ were 20% lower than for RH <5%.

Correlation of load-displacement curves with SEM images before splitting revealed a humidity-dependent sensibility of the fracture toughness to the presence of surface flaws. Fig. 3f elucidates the observed behavior: for tests at RH >60%, surface defects had a detrimental effect, reducing K_c by up to 41% compared to the most pristine specimens; in contrast, surface defects only caused minor scatter in the fracture toughness at RH <5%. However, pristine specimens reached similar K_c for both RH <60% and RH <5%. These results were consistent over more than 5 pillars tested for each RH.

Our results well corresponded to previously reported micro-pillar compression measurements [11,12,15], demonstrating good transferability between different characterization approaches. We found that the fracture toughness of TPP-DLW-derived pyrolytic carbon, with average values of 2.3-2.8 MPam$^{0.5}$, was up to 500% higher than that of macroscopic forms of vitreous carbon, which typically lies in the range of 0.5-1.4 MPam$^{0.5}$ [25,33,35]. Specimens in this work were completely amorphous, absent of STEM-detectable internal defects and showed only a limited presence of surface flaws. In contrast, macroscopic pyrolytic carbon is usually characterized by a significantly higher flaw distribution, as well as a nanoporous microstructure with small layered (graphite-like) [26,35] or core-shell [36] domains, that induce anisotropy in the fracture toughness. Therefore, the found toughness increase is expected. It should be noted though, that the numerical values in this study may be subject to a certain quantitative uncertainty from the coefficient γ in Eq. (1), which only accounts for radial cracks (either Palmqvist-like or median/radial). Since median cracks clearly dominated the experimental behavior, as confirmed by the FIB cross-section, γ values may sufficiently well represent the materials behavior, though, despite not considering the observed smaller surface ring cracks, which are characteristic of pyrolytic glassy carbon [34]. Also, it is emphasized that the observed crack geometry (Fig. 3b and c) was throughout this study consistent and the ratios

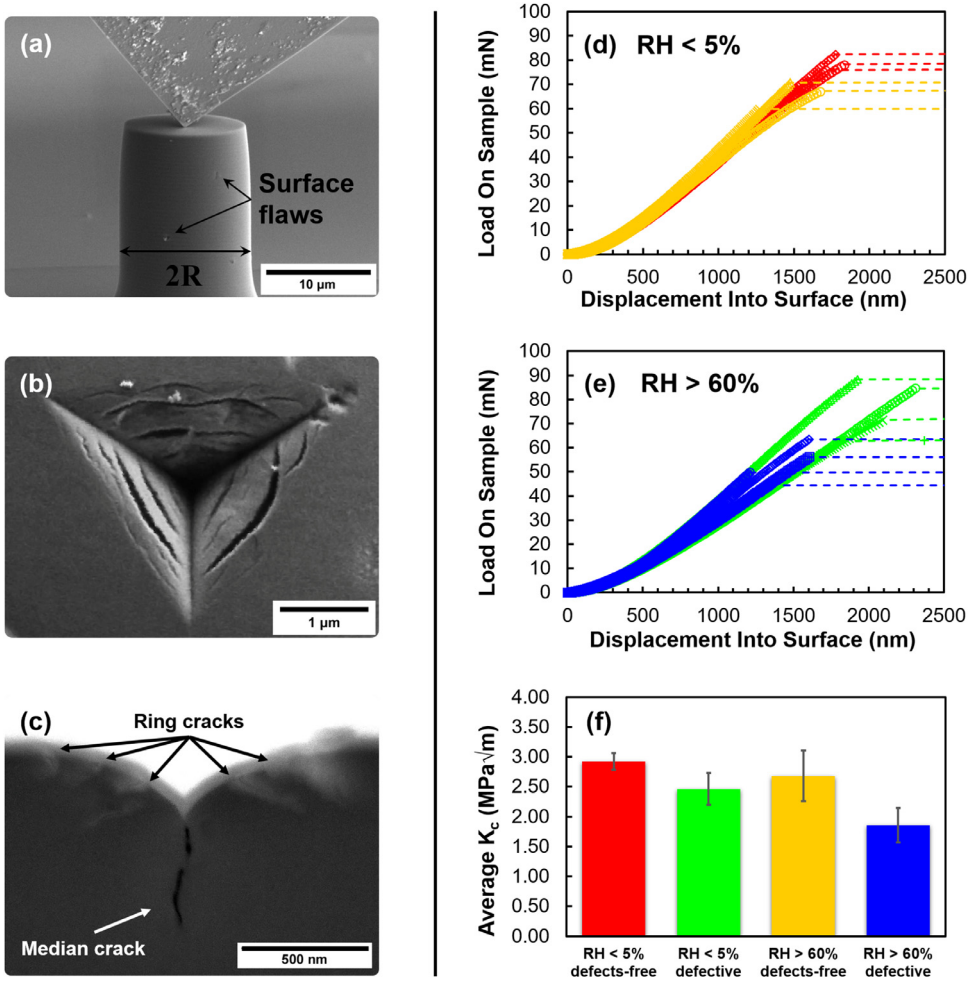

Fig. 3. (a) Representative arrangement of the pillar splitting testing procedure on a pyrolytic carbon micro-pillar with surface flaws. Observed (b) surface morphology and (c) FIB cross-section of the indent just before splitting failure. Representative load-displacement curves at a relative humidity (RH) of (d) <5% and (e) >60%. (e) average fracture toughness comparison at the two RH ranges for pristine and defected pillars (colors in Fig. 3f correspond to colors in Fig. 3d and e).

between the found toughness values under different conditions are hence quantitatively valid.

Being based on the interaction between internally propagating cracks and the free surface, pillar splitting is able to to detect sensitivity of the fracture toughness to surface conditions, such as residual stress and defects. Recently, splitting of FIB-milled micro-pillars has been used to measure diameter-dependent toughening from FIB-induced residual stress on the external surface of the pillars [32].

According to a previous study [37], the dependency of of a semi-elliptical crack approaching a free surface can be described by a stress intensity magnification factor (K_I) modifying the semi-infinite stress intensity factor:

$$K_I = \frac{A}{1-\frac{c}{R}} \cdot \frac{F}{c^{3/2}} \tag{2}$$

where $\boldsymbol{c}$ is the crack length, $\boldsymbol{F}$ is the applied force, $\boldsymbol{R}$ is the pillar radius and $\boldsymbol{A}$ is a constant that may change depending on the surface conditions of the pillar. Surface cracks and chemically induced weakening, such as associated to water diffusion, contribute to A and thus K_I, promoting early splitting failure. Given the statistical nature of this phenomenon, it is expected that the main effects on experimental results would be the increase of scattering of the data when testing at higher humidity levels. In support of this hypothesis, (i) the fracture toughness of specimens without surface flaws was observed to be independent of the testing humidity and (ii) the absence of water despite the presence of surface flaws did not cause as pronounced toughness knockdowns.

The found sensitivity to the environmental humidity of the fracture toughness of TPP-DLW-derived pyrolytic carbon may be explained by a scale-dependent interplay between the RH-level and the flaw distribution of the material. With water contact angle values in the range of 50-70° [38,39], pyrolytic carbon and similar materials are reported hydrophilic, suggesting that at elevated humidity, the presence of surface flaws allows water diffusion into the material of our micro-pillar specimens (Fig. 4). Chemical reactions between water and the glassy carbon may have induced local weakening of the material, functioning as a stress intensity magnification factor during the pillar splitting experiments, similarly as reported previously for silica and soda-lime glasses [40,41]. However, humidity sensitivity has not been reported in macroscopic pyrolytic carbon although it typically contains a considerably higher population of notably larger flaws than the specimens of this study, which should promote diffusion. Although seemingly counterintuitive the humidity sensitivity in this study may be related to a size-effect: at small scales, increased surface-to-volume ratios amplify detrimental surface effects. Even though decreasing flaw size is well known to enhance toughness, the effects of chemical surface modifications may be expected to increase with smaller specimen size as well. Capillary pressure from the enclosed water may additionally have caused a change in the stress distribution around the surface flaws. However, this effect is less clear, since

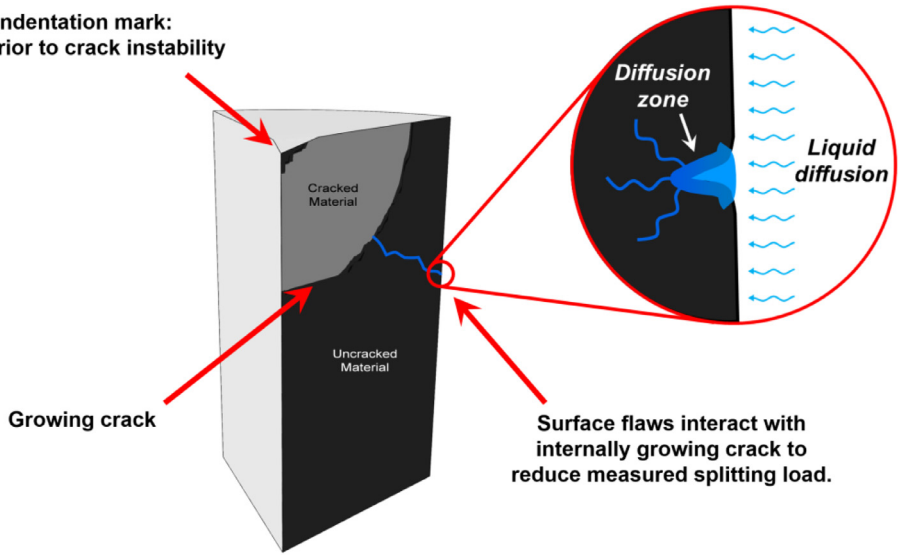

Fig. 4. Interaction mechanism between indentation induced main crack and surface flaws to increase stress intensity magnification factor and, consequently, reduce the critical splitting load.

swelling-induced stress could also increase the fracture resistance [42,43].

This study demonstrates that fracture toughness in additively manufactured nano-ceramics is, in contrast to macroscopic ceramics, a surface dominated characteristic, where processing-induced cavities and nano-porosity can have a paramount effect on reliability and durability. Different humidity conditions represent a ubiquitous boundary condition for almost any application. Consequently, toughening material design in micro- and nano-architected metamaterials and devices will need to have a strong focus on surface effects like the found capillary embrittlement. The observed humidity effect can have a remarkable impact on the scale-up of such architected materials in a wide range of applications, especially in biomedical and micro-fluidics fields.

Declaration of Competing Interest

The authors declare that they have no known competing financial interests or personal relationships that could have appeared to influence the work reported in this paper.

Acknowledgment

M.S. and E.R. gratefully acknowledge partial financial support from the European Commission, European project Oyster, grant agreement n. 760827.

Supplementary materials

Supplementary material associated with this article can be found, in the online version, at doi:10.1016/j.scriptamat.2020.113684.

References

[1] J. Bauer, A. Schroer, R. Schwaiger, O. Kraft, Nat. Mater. 15 (2016) 438–443.
[2] T. Baldacchini, Three-Dimensional Microfabrication Using Two-Photon Polymerization, first ed., Elsevier, Amsterdam, 2015.
[3] J.K. Hohmann, M. Renner, E.H. Waller, G. von Freymann, Adv. Opt. Mater. 3 (2015) 1488–1507.
[4] G. von Freymann, A. Ledermann, M. Thiel, I. Staude, S. Essig, K. Busch, M. Wegener, Adv. Funct. Mater. 20 (2010) 1038–1052.
[5] J. Bauer, L.R. Meza, T.A. Schaedler, R. Schwaiger, X. Zheng, L. Valdevit, Adv. Mater. 29 (2017) 1701850.
[6] A. Marino, O. Tricinci, M. Battaglini, C. Filippeschi, V. Mattoli, E. Sinibaldi, G. Ciofani, Small 14 (2018) 1702959.
[7] T. Gissibl, S. Thiele, A. Herkommer, H. Giessen, Nat. Photonics 10 (2016) 554–560.
[8] G. Nelson, R.A. Kirian, U. Weierstall, N.A. Zatsepin, T. Faragó, T. Baumbach, F. Wilde, F.B.P. Niesler, B. Zimmer, I. Ishigami, M. Hikita, S. Bajt, S.-R. Yeh, D.L. Rousseau, H.N. Chapman, J.C.H. Spence, M. Heymann, Opt. Express 24 (2016) 11515.
[9] C. Yang, Q. Cao, P. Puthongkham, S.T. Lee, M. Ganesana, N.V. Lavrik, B.J. Venton, Angew. Chem. Int. Ed. 57 (2018) 14255–14259.
[10] H. Cui, R. Hensleigh, H. Chen, X. Zheng, J. Mater. Res. 33 (2018) 360–371.
[11] A. Guell Izard, J. Bauer, C. Crook, V. Turlo, L. Valdevit, Small 15 (2019) 1903834.
[12] C. Crook, J. Bauer, A. Guell Izard, C. Santos de Oliveira, J. Martins de Souza e Silva, J.B. Berger, L. Valdevit, Nat. Commun. 11 (2020) 1579.
[13] Z.C. Eckel, C. Zhou, J.H. Martin, A.J. Jacobsen, W.B. Carter, T.A. Schaedler, Science 351 (2016) 58–62.
[14] J. Bauer, C. Crook, A. Guell Izard, Z.C. Eckel, N. Ruvalcaba, T.A. Schaedler, L. Valdevit, Matter 1 (2019) 1–10.
[15] A. Albiez, R. Schwaiger, MRS Adv. 4 (2019) 133–138.
[16] Y. Ji, C. Li, G. Wang, J. Koo, S. Ge, B. Li, J. Jiang, B. Herzberg, T. Klein, S. Chen, J.C. Sokolov, M.H. Rafailovich, EPL 84 (2008) 56002.
[17] J. Bauer, A. Guell Izard, Y. Zhang, T. Baldacchini, L. Valdevit, Adv. Mater. Technol. 4 (2019) 1900146.
[18] J. Bauer, A. Guell Izard, Y. Zhang, T. Baldacchini, L. Valdevit, Opt. Express 28 (2020) 20362–20371.
[19] J.S. Oakdale, J. Ye, W.L. Smith, J. Biener, Opt. Express 24 (2016) 186–194.
[20] N. Rohbeck, R. Ramachandramoorthy, D. Casari, P. Schürch, T.E.J. Edwards, L. Schilinsky, L. Philippe, J. Schwiedrzik, J. Michler, Mater. Des. 195 (2020) 108977.
[21] S.M. WIEDERHORN, J. Am. Ceram. Soc. 50 (1967) 407–414.
[22] B. Lawn, Fracture of Brittle Solids, second ed., Cambridge University Press, 1993, doi:10.1017/CBO9780511623127.
[23] A. Koike, M. Tomozawa, J. Non. Cryst. Solids 352 (2006) 5522–5530.
[24] K. HIRAO, M. TOMOZAWA, J. Am. Ceram. Soc. 70 (1987) 377–382.
[25] W.P. Minnear, T.M. Hollenbeck, R.C. Bradt, P.L. Walker, J. Non. Cryst. Solids 21 (1976) 107–115.
[26] J.S. NADEAU, J. Am. Ceram. Soc. 57 (1974) 303–306.
[27] D. Gailevičius, V. Padolskytė, L. Mikoliūnaitė, S. Šakirzanovas, S. Juodkazis, M. Malinauskas, Nanoscale Horiz. 4 (2019) 647–651.
[28] M. Sebastiani, K.E. Johanns, E.G. Herbert, F. Carassiti, G.M. Pharr, Philos. Mag. 95 (2015) 1928–1944.
[29] M. Ghidelli, M. Sebastiani, K.E. Johanns, G.M. Pharr, J. Am. Ceram. Soc. 100 (2017) 5731–5738.
[30] M.Z. Mughal, R. Moscatelli, H.Y. Amanieu, M. Sebastiani, Scr. Mater. 116 (2016) 62–66, doi:10.1016/j.scriptamat.2016.01.023.
[31] Nanoscribe GmbH & Co. KG, Photonic Professional (GT) User Maual, 2017.
[32] C.M. Lauener, L. Petho, M. Chen, Y. Xiao, J. Michler, J.M. Wheeler, Mater. Des. 142 (2018) 340–349.
[33] J.X. Zhao, R.C. Bradt, P.L.J. Walker, Carbon 23 (1985) 15–18.
[34] M. Sakai, H. Hanyu, M. Inagaki, J. Am. Ceram. Soc. 78 (1995) 1006–1012.
[35] M. Sakai, R.C. Bradt, D.B. Fischbach, J. Mater. Sci. (1986).
[36] K. Kawamura, G. Jenkins, J. Mater. Sci. 5 (1970) 262–267.
[37] R.C. Shah, A.S. Kobayashi, Int. J. Fract. 9 (1973) 133–146.

[38] A. Kozbial, Understanding the Intrinsic Water Wettability of Graphite, University of Pittsburgh, Swanson School of Engineering, 2010.
[39] R.C. Engstrom, V.A. Strasser, Anal. Chem. 56 (1984) 136–141.
[40] R.J. Charles, J. Appl. Phys. 29 (1958) 1549, doi:10.1063/1.1722991.
[41] T.A. Michalske, S.W. Freiman, Nature 295 (1982) 511–512.
[42] S.M. Wiederhorn, T. Fett, G. Rizzi, S. Fünfschilling, M.J. Hoffmann, J.-P. Guin, J. Am. Ceram. Soc. 94 (2011) s196–s203, doi:10.1111/j.1551-2916.2011.04530.x.
[43] S.M. Wiederhorn, T. Fett, G. Rizzi, M.J. Hoffmann, J.-P. Guin, Metall. Mater. Trans. A 44 (2013) 1164–1174.